Original Research

Optimization and Modelling Using the Response Surface Methodology for Methylene Blue Removal by Electrocoagulation/Hazelnut Shell Adsorption Coupling in a Batch System

Mijia Zhu*, Xianqing Yin, Qian Liu, Zhiyun Feng

School of Chemistry and Environmental Engineering, Yangtze University, Jingzhou, P.R. China

Abstract

The present work examined the removal of methylene blue (MB) from aqueous solutions through an electrocoagulation/hazelnut shell (EC/HNS) adsorption coupling process. The process was evaluated using a Box–Behnken design (BBD) under the response surface methodology (RSM). According to the obtained results from BBD–RSM regression analysis, we found that the experimental data are best fitted to the second-order polynomial model with coefficient of determination (R^2) value of 0.9534, adjust coefficient (R_{adj}^2) value of 0.9926 and predicted correlation coefficient (R_{Pred}^2) value of 0.9973. The maximum MB removal efficiency was obtained under optimized conditions (HNS dosage, 6 g/L; reaction time, 17.75 min; and current density, 2.6 mA/cm^2). Under the optimum conditions, the MB removal rate reached 99.45%, and the RSM predictive value was 98.71% with a small deviation. These results confirmed that the RSM model accurately and reliably analysed the process of removing MB from wastewater.

Keywords: electrocoagulation, hazelnut shell, Methylene Blue, adsorption, response surface methodology
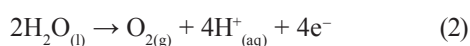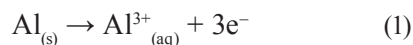
Introduction

Water pollution due to rapid industrialisation and urbanisation is a real threat. Wastewater discharged by the textile industry contains toxic compounds and is thus a major global problem [1]. The release of dyes into water is harmful to human health and natural ecosystems due to their toxic, carcinogenic, mutagenic and teratogenic effects [2]. Methylene blue (MB) is one of the most commonly used dyes in the textile and paper industries [3]. MB can move through effluent during production and affect the quality of water due to its high water solubility [4]. Thus, MB must be removed from aqueous solution for the protection of the environment and human health. Various approaches have been adopted for wastewater treatment, including filtration [5], nonthermal plasma [6], electrocatalytic oxidation [7], Fenton-like oxidation [8], photodegradation [9, 10] and ultrasonic degradation [11]. However, these processes
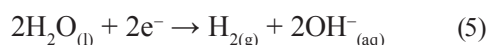
*e-mail: zhumijia128@163.com

are either inefficient or expensive. Thus, increased attention is being paid to combination processes such as electrocoagulation (EC) and adsorption [12-14].

EC is attracting significant attention as a highly efficient technology for wastewater treatment [12]. The process is characterised by the in situ electrogeneration of coagulants. According to the EC mechanism, coagulants are generated via electrolytic oxidation of a soluble anode, which is usually aluminium or iron [15]. In the case of EC with Al, the reactions occurring at the anode are as follows:

$$Al_{(s)} \rightarrow Al^{3+}_{(aq)} + 3e^- \qquad (1)$$

$$2H_2O_{(l)} \rightarrow O_{2(g)} + 4H^+_{(aq)} + 4e^- \qquad (2)$$

$$Al^{3+}_{(aq)} + 3H_2O_{(l)} \rightarrow Al(OH)_{3(aq)} + 3H^+_{(aq)} \qquad (3)$$

$$n\ Al(OH)_{3(aq)} \rightarrow Al_n(OH)_{3n(aq)} \qquad (4)$$

The reaction at the cathode is written as:

$$2H_2O_{(l)} + 2e^- \rightarrow H_{2(g)} + 2OH^-_{(aq)} \qquad (5)$$

Al^{3+} ion generation occurs at the anode surface, whereas hydrogen gas transpires at the cathode surface. Flocs of Al(III) hydroxides and polyhydroxy species formed during coagulation, and the organic pollutants are removed from the aqueous phase via charge neutralisation, adsorption and sweep flocculation [16]. The flocs can then be separated by sedimentation or/and flotation [12].

The advantages of EC include ease of operation, minimum requirements for chemical use, low sludge production, short operation time and high pollutant removal efficiency [17, 18]. However, Avsar et al. found ease in forming an impermeable oxide film on the cathode surface, leading to increased energy consumption and decreased efficiency [19]. A possibility to improve EC progress has been suggested by Vivek and Ganesan [20]. In their study, granular active carbon/EC coupling technique was proven to be more efficient and faster compared with conventional EC in wastewater treatment. Similar to active carbon, hazelnut shell (HNS) is also a potential adsorbent with well-developed porosity and large internal specific area. As an effective wastewater treatment method, HNS adsorption has been reported in various studies, such as removal of dyes and heavy metal ions from aqueous solution [2, 21-24]. Moreover, HNS is an agricultural waste present in large amounts in northern China. HNS can also be used for MB removal from wastewater by an EC/HNS adsorption coupling system. To the best of our knowledge, a few studies have focused on MB removal from aqueous solution using the EC/HNS adsorption coupling method.

The effect of current density, reaction time and adsorbent dosage on MB removal efficiency was investigated in this work to determine the optimum

Table 1. Characterization of HNS.

Property	Value
Iodine value	900 mg/g
Moisture	$\leq 2\%$
Ash	$\leq 5\%$
S_{BET}	752 m²/g
V_{total}	67.2 cm³/g
V_{micro}	0.35 cm³/g

operational parameters in the wastewater treatment system because most previous studies were based on a one-factor-at-a-time method [12, 14, 20, 25]. In the current study, response surface methodology (RSM) was used to evaluate the effects of two or more independent variables on the dependent variable to achieve the optimum condition for the EC/HNS adsorption coupling process.

Experimental

Materials

HNS was collected from Hebei Province, China. The agricultural residues (HNS) were boiled in deionised water for 1 h and then washed with deionised water three to five times. The samples were treated under a nitrogen flow rate of 100 cm³/min at 300ºC for 30 min. Afterwards, the dried slices were ground and sieved, and a particle size fraction of 0.4-3.0 mm was then used. The quality testing indices of HNS were described in Table 1 based on the National Standard of China for Nut Shell Activated Carbon Testing (GB/T 7702-1997). The specific surface areas were calculated from the N_2 isotherm data by the Brunauer-Emmett-Teller equation. Pore distributions were measured by N_2 isotherm data using nonlocal density functional theory. The physical properties and chemical composition of the HNS before and after MB uptake were investigated under the adsorption conditions (initial MB concentration: 50 mg/L, HNS dosage: 10 g/L, pH: 7). The samples were dried at room temperature and coated with Au under vacuum in an argon atmosphere for the
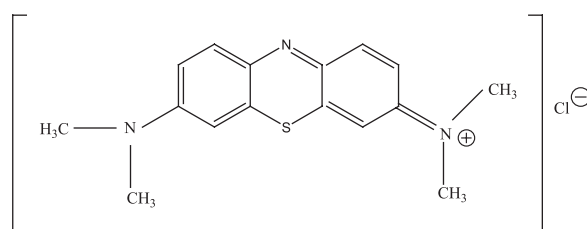

Fig. 1. Chemical structure of Methylene Blue.

SEM-EDX studies (SU8010, Hitachi, Tokyo, Japan). The FTIR spectrum of the HNS was calculated in the range of 4000 cm^{-1} to 400 cm^{-1} using a Perkin Elmer Model spectrum 400 FTIR/FTNIR spectrometer with deuterated triglycine sulfate detector and KBr beam splitter.

A cationic dye MB ($C_{16}H_{18}ClN_3S$, MW = 319.90 g/mol) was purchased from Labest Bio–Technology Co., Ltd (Beijing, China). The chemical structure is presented in Fig. 1. The EC/HNS adsorption coupled process was carried out in a batch model. A total of 1000 cm^3 of 50 mg/L MB solution was placed in the experimental cell in each run. A weight of 1 g NaCl (purity≥99.5%, Keephway Co., Ltd, Beijing, China) was dissolved in dye solutions (1000 cm^3) to adjust the solution conductivity.

Experimental Procedure

The EC reactor comprised a parallel-plate EC cell provided with two facing electrodes. The experimental setup used in this study is shown in Fig. 2. The effective area of each electrode plate was 90 cm^2. The anode and cathode were positioned vertically and fixed at 1 cm away from each other. The electrodes were aluminium (Al, anode) and stainless steel (SS, cathode) connected to a digital direct current power supply (WKY-505, East Co., Ltd, Guangdong, China) with a voltage and an electrical current range of 0-50 V and 0-5 A. The electrodes were rubbed with fine-grained emery paper and washed with 1 N H_2SO_4 and distilled water before each run. All the runs were performed at room temperature of 20±1°C. At the end of the experiments, samples were filtrated using Whatman 0.45 μm filters and then analysed.

Analytical Method

The MB concentration was determined by spectrophotometry (UV-1800 UV/VIS spectrophotometer, Shimadzu Co., Ltd, Kyoto, Japan). The concentration was determined using the initial calibration curve, which was recorded after spectrophotometric measurement of the solution adsorbance for MB standard concentration at
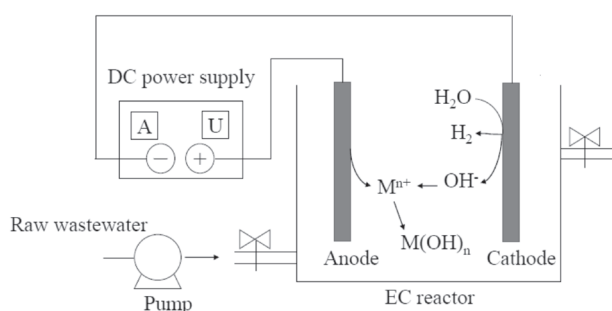
Table 2. Experimental ranges and levels of the independent variables.

Name of variables	Range and level		
	−1	0	+1
Dosage (g/L)	4	5	6
Reaction time (min)	10	15	20
Current density (mA/cm^2)	2	2.5	3

the specific wavelength (665 nm) corresponding to the maximum absorption of dye. The MB removal efficiency (Y, %) was calculated from the following equation:

$$Y = (C_0 - C_t)/C_0 \times 100\% \qquad (6)$$

…where C_0 (mg/L) is the concentration of MB before EC/HNS process and C_t (mg/L) is the concentration of MB after t min of EC/HNS process.

RSM Experimental Design and Statistical Analysis

The Box-Behnken design (BBD), a standard RSM, was selected for the optimization of the factors, which made sense for MB removal efficiency. In this design, three factors were the dosage of HNS (X_1), reaction time (X_2) and current density (X_3), respectively (Table 2). All factors were controlled at three levels. The experimental design consists of 15 experiments with 3 centre points (to allow estimation of pure error). All the experiments were performed in triplicate, and the MB removal efficiency was considered as the response. A non-linear regression method was used to fit the second-order model inthe form of quadratic polynomial equation:

$$Y = \beta_0 + \sum_{i=1}^{k} \beta_i x_i + \sum_{i=1}^{k} \beta_{ii} x_i^2 + \sum_{i=1}^{k} \sum_{j=1}^{k} \beta_{ij} x_i x_j + \varepsilon$$

$$\qquad (7)$$

… where Y is the response; β_0 is a constant coefficient; ε is the error; and β_i, β_{ii} and β_{ij} are interaction coefficients of linear, quadratic and second-order terms, respectively. x_i and x_j are independent variables which determine Y. The subscripts i and j are the integer variables. The quality of the fit and the significance of the model were checked with the coefficient of determination (R^2) and Fisher's F-test, which were performed by analysis of variance (ANOVA) with 95% confidence level. After fitting the response surface model, a numerical optimization technique (Derringer's desired function methodology) was introduced to evaluate the optimal operating conditions. All statistical analyses were performed using Design Expert 8.0 software (Stat Ease Inc., Minneapolis, USA).
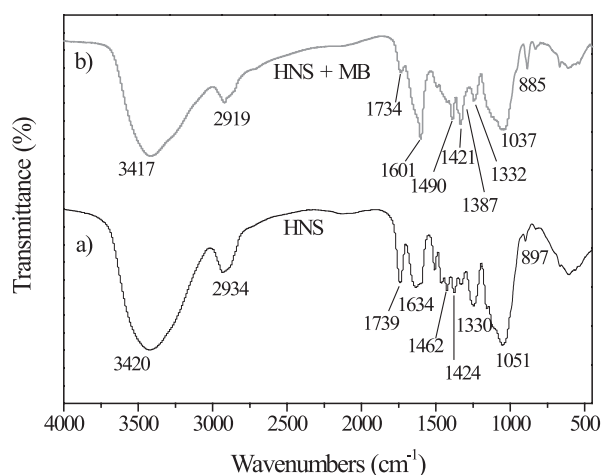

Fig. 2. Electrocoagulation system.

Fig. 3. FTIR spectra of the hazelnut shell before a) and after b) Methylene Blue adsorption.

Results and Discussion

Characterization of HNS

The FTIR spectra of HNS were taken before and after MB adsorption to ascertain the interaction between the HNS surface and dye molecules (Fig. 3).

From Fig. 3a), the strong vibration and broadband at approximately 3500-3000 cm^{-1} is characteristic of –OH stretching vibrations, thereby showing that HNS surface has numerous alcoholic and phenolic –OH groups. Bands appearing at 2934, 1739, 1634, 1424, 1051 and 897 cm^{-1} were assigned to C–H stretching of alkane, C=O stretching of carboxylic acid or ester, COO$^-$ anion stretching, CH$_2$ bending, C–O stretching of ester or ether and N–H deformation of amines, respectively [26]. Fig. 3b) reveals that a few bands were shifted, and a few new bands appeared after MB adsorption. The bands at 3420, 2934, 1739, 1634, 1424, 1051 and 897 cm^{-1} were shifted to 3417, 2919, 1734, 1601, 1421, 1037 and 885 cm^{-1}, respectively, after MB adsorption. The bands at 1490, 1387 and 1332 cm^{-1} can be attributed to >S=O groups of sulfonamides and thioester [27]. FTIR analysis showed that OH, C–H, C=C, C=O and carbonyl groups on the HNS surface are involved in the adsorption of MB.

The SEM image of HNS before adsorption (Fig. 4a) shows that the surface of HNS is irregular and porous. After adsorption, the agricultural residues have a rough surface because they are partially covered by MB molecules (Fig. 4b). Elemental analysis was conducted with the use of EDX to determine the composition of HNS. The EDX analysis of unadsorbed HNS (Fig. 4c) indicates that Si was evident at peak position.
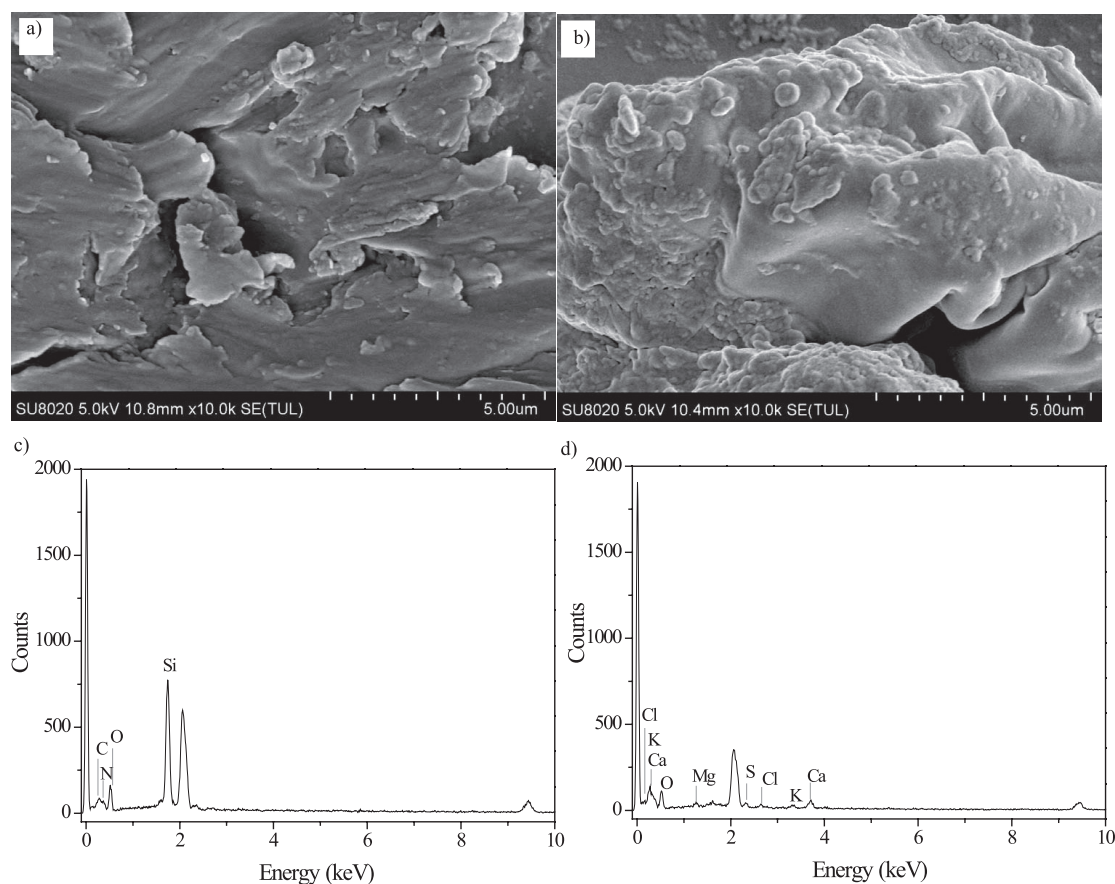

Fig. 4. Scanning electron microscopic (SEM) and energy dispersive X-ray (EDX) analysis of a), c) unadsorbed and b), d) MB-adsorbed hazelnut shell.

Table 3. Design matrix in coded units and the experimental response.

Run number	Dosage (X_1)	Reaction time (X_2)	Current density (X_3)	Removal efficiency (%, Y)
1	−1	1	0	90.2
2	−1	−1	0	54.1
3	0	−1	1	66.3
4	1	0	−1	82.2
5	1	0	1	93.2
6	1	1	0	93.7
7	0	0	0	91.5
8	−1	0	1	89.0
9	0	0	0	92.2
10	−1	0	−1	76.5
11	0	1	−1	83.4
12	0	−1	−1	46.2
13	0	0	0	90.9
14	0	1	1	92.4
15	1	−1	0	60.5

After MB adsorption, the EDX (Fig. 4d) showed the presence of S due to the trapped dye molecules containing sulfonic groups, thereby confirming the adsorption phenomenon.

Statistical Analysis and Regression Model

A total of 15 designed batch runs of experimental conditions, including 3 central points, were derived from BBD. The experiments were conducted in triplicate to obtain different combinations of the process parameters using statistically designed experiments. The various combinations of experimental conditions with their responses are presented in Table 3.

The obtain the 'goodness of fit', ANOVA was used to analyze the data from this study. The MB removal model was significant by the F-test at the 95% confidence level (prob>F<0.05). The following fitted regression models (Eq. 8), were obtained to quantitatively ascertain the effects of the input variables on MB removal:

$$Y = 91.53 + 2.47X_1 + 16.58X_2 + 6.57X_3 - 0.72X_1X_2$$
$$-0.37X_1X_3 - 2.77X_2X_3 - 1.88X_1^2 - 15.03X_2^2 - 4.43X_3^2$$
(8)

The ANOVA test for the MB removal model (Table 4) showed that the model's F value was 209.88, thereby implying that the model was significant. The probability of a large F value due to the uncontrollable noise factors was observed to be less (<0.01%). A p value less than 0.05 indicated that the model terms X_1, X_2, X_3, X_2X_3, X_1^2, X_2^2 and X_3^2 were significant.

Fig. 5a) shows a plot revealing the normal probability of the Student's t test residuals for MB removal efficiency. The plot is an important diagnostic tool to check model adequacy. Most of the obtained data points follow a straight line, thereby suggesting that the data were normally distributed in the responses of the model. The coefficient of determination (R^2) is defined as the ratio of the predicted variation. The high R^2 value of 0.9534 showed a small difference between the predicted and actual values of the response. The value of the adjusted determination coefficient ($R_{adj}^2 = 0.9926$) in the regression model was also close to 1, thereby indicating that the experimental values can be significantly predicted by the model (in Table 4). Moreover, the predicted versus actual value plot of the response surface model presented in Fig. 5b) revealed excellent agreement ($R_{Pred}^2 = 0.9973$) between the actual and predicted data obtained from the model. Therefore, the results indicate that the second-order polynomial model is statistically valid.

Interactive Effect of the Process Variables

2D response surface contour plots were derived based on the mathematical regression model to obtain new insights into the interaction effect between the independent variables on MB removal efficiency. Fig. 6a) describes the interaction between the dosage and reaction time with a current density of 2.5 mA/cm². At 4 g/L, the removal efficiency increased by 38.23% (from 54.1% to 92.33%) and then decreased by 2.13% (from 92.33% to 90.2%) when the time increased from 10 min to 20 min; whereas at 6 g/L, the
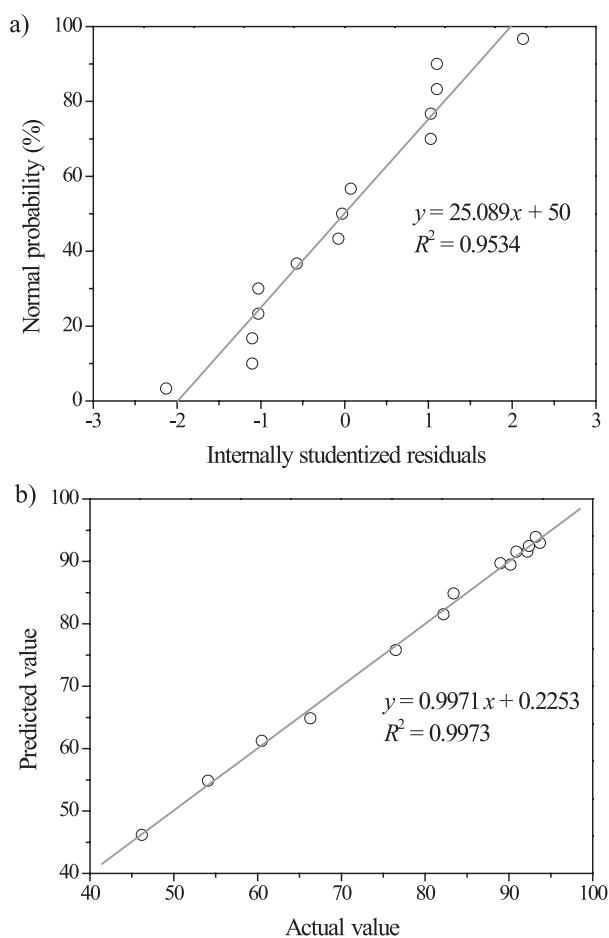
a)

b)

Fig. 5. Normal probability plot of the internally studentized residuals a) and predicted vs. actual values plot b) in the response surface model.

removal efficiency increased by 35.85% (from 60.5% to 96.35%) and then decreased by 2.65% (from 96.35% to 93.7%) when the reaction time increased from 10 min to 20 min. This finding can be attributed to the increasing sorption surface and binding sites in the adsorbent to the MB adsorption by increasing the dose. In the study conducted by Yang et al., cellulose nanocrystal from *Carex meyeriana* Kunth was used to remove MB from aqueous solutions [28]. Removal efficiency showed an increasing trend from 90.85%±2.34% to 98.76%±2.21%, with an increasing adsorbent dosage from 15 mg to 30 mg. However, when the dosage was achieved at a certain value, the number of adsorption sites on the adsorbent was larger than the number of MB, thereby preventing further increases in removal efficiency. The enhancement of dosage augments the diffusional path length and decreases the surface area by agglomeration of sorbent particles. Moreover, abundant sites of the adsorbent may be blocked due to high dosage [29].

The interaction between dosage and current density at a reaction time of 15 min is illustrated in Fig. 6b). The plot shows that the removal efficiency increased by 13.45% (from 76.5% to 89.95%) and then decreased by 0.95% (from 89.95% to 89%) at the dosage of 4 g/L, whereas that at dosage of 6 g/L increased by 12.12% (from 82.2% to 94.32%) and then decreased by 1.12% (from 94.32% to 93.2%) when the current density increased from 2 mA/cm^2 to 3 mA/cm^2. The MB removal efficiency also increased as a function of current density. According to Faraday's Law, the amount of monomeric and polymeric species of Al grows by increasing the current density. The high

Table 4. ANOVA for response function and variables selected to fit a model.

Source	Sum of Squares	df	Mean Square	*F* value	*p*-value Prob>*F*
Model	3500.85	9	388.98	209.88	<0.0001
X_1	49.01	1	49.01	26.44	0.0036
X_2	2197.84	1	2197.84	1185.89	<0.0001
X_3	345.85	1	345.85	186.61	<0.0001
X_1X_2	2.10	1	2.10	1.13	0.3355
X_1X_3	0.56	1	0.56	0.30	0.6054
X_2X_3	30.80	1	30.80	16.62	0.0096
X_1^2	13.04	1	13.04	7.04	0.0453
X_2^2	834.00	1	834.00	450.00	<0.0001
X_3^2	72.43	1	72.43	39.08	0.0015
Residual	9.27	5	1.85		
Lack of Fit	8.42	3	2.81	6.63	0.1339
Pure Error	0.85	2	0.42		
Cor Total	3510.12	14			

$R^2 = 0.9974$, $R_{adj}^2 = 0.9926$

amounts of generated coagulant can enhance MB removal efficiency. Using aluminium as an electrode material results in the formation of passive oxide film, which inhibits the EC process. This condition is the potential reason for such a slight decline in the MB removal percentage when the current density exceeds a certain value. A similar phenomenon is reported by Zhu et al. [30].

Fig. 6c) illustrates the combined effects of reaction time and current density when the dosage was at zero

(5 g/L). At a current density of 2 mA/cm², the removal efficiency increased (from 46.2% to 87.21%) when the reaction time increased from 10 min to 17.9 min and then decreased (from 87.21% to 83.4%) until 20 min; at a current density of 3 mA/cm², the removal efficiency increased (from 66.3% to 96.73%) when the reaction time increased from 10 min to 17.9 min and then decreased (from 96.73% to 92.4%) until 20 min. This result may be attributed to the abundantly available unsaturated sites on the surface of the adsorbent at the beginning of the reaction time. The adsorption became slow with a further increase in time due to the decrease in the number of active surface area [31].

Optimization and Model Validation

The desirable point prediction function in the experimental design was applied to identify the optimum conditions to maximise MB removal efficiency within the studied experimental ranges. At the laboratory scale, the maximum removal efficiency of 99.45% was obtained at a dosage of 6 g/L, reaction time of 17.75 min and current density of 2.6 mA/cm². Experiments were operated under the optimum conditions and the five other predicted conditions to test the validity of the model. MB removal results are described in Table 5. The actual results are closely related with the predicted data with a low percentage of error (0.88, −1.35, 1.10, −0.82, −1.63 and 0.75), thereby indicating the suitability of the developed model.

Economic and Technical Analysis

The calculated cost of current, voltage and reaction time was considered in the assessment of the described EC/HNS coupled system. In this study, current density and reaction time at the optimum operating conditions were 2.6 mA/cm² and 17.75 min, respectively. For this current density, current and voltage values were 0.468 A and 7.5 V, respectively. Based on these values, the energy consumption (ENC) can be estimated by the following equation:

$$ENC = (UIt)/v \qquad (9)$$

…where U, I, t and v are the voltage (V), current (A), reaction time (h) and effluent volume (m³), for the EC process. Based on the China market in 2018, the electricity cost was \$0.049/kwh. The cost of EC was estimated as \$2.88/m³ for MB water treatment.

Table 6 lists the performances of the EC/HNS coupling system under optimized conditions and the former EC technologies. Considering its high removal efficiency and short reaction time, EC/HNS is a potential technique in the cleaning of MB wastewater.
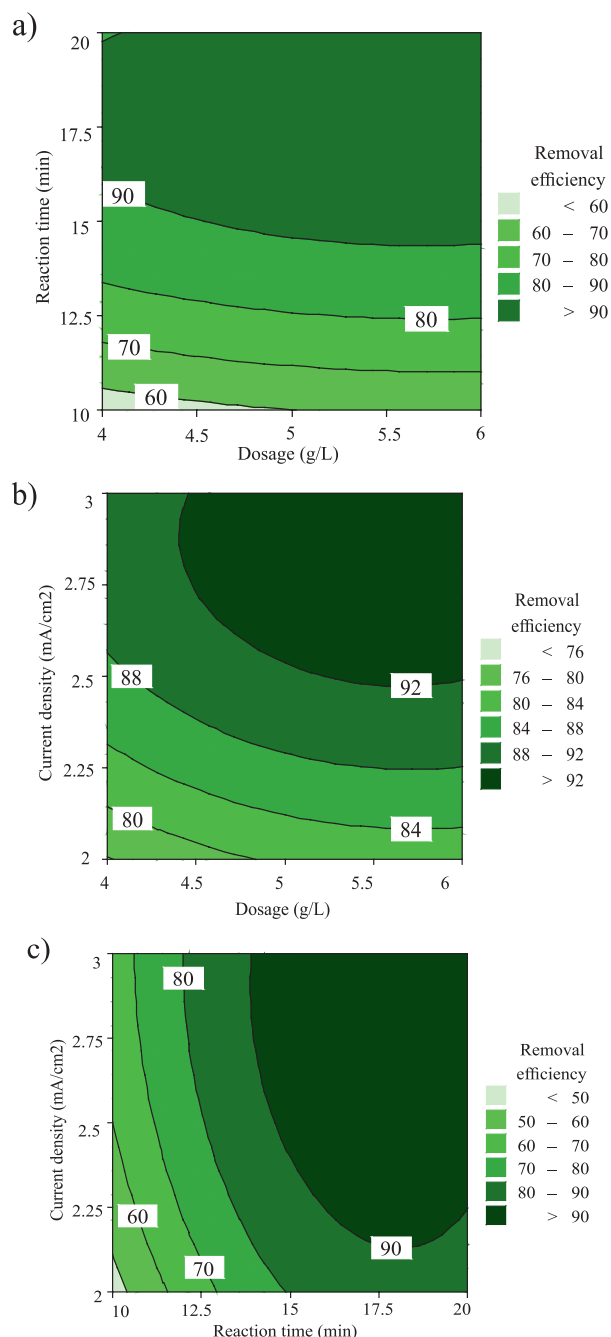

Fig. 6. Response surface plots for interactive effect among factors a-c): dosage and reaction time; dosage and current density; current density and reaction time) on Methylene Blue removal efficiency.

Table 5. Verification test of the fitting model.

Test number	Operation parameter			Y (%)		
	X_1	X_2	X_3	Observed value	Predicted value	% Error
1	1	−0.46	−0.86	72.45	71.82	0.88
2	1	0.1	0.67	94.27	95.56	−1.35
3	0.25	−1	0.27	63.42	62.73	1.10
4	0.5	0.95	−0.85	73.71	74.32	−0.82
5	0.72	−0.12	0.36	76.89	78.70	−1.63
Optimal condition	1	0.55	0.21	99.45	98.71	0.75

Table 6. Comparison of EC/HNS and other different EC systems for MB removal.

Initial MB concentration (mg/L)	Removal efficiency	Operational parameters	Reference
20	89%	Current intensity 3 A, Reaction time 40 min, Fe–Fe	[32]
50	95.78%	Current density 50 mA/cm², Reaction time 24 min, Al–Fe, pH 9	[33]
50	95.5%	Current density 150 mA/cm², Reaction time 20 min, Fe–Fe, pH 6.5	[34]
50	93%	Current density 30 mA/cm², Reaction time 15 min, NaCl concentration 6 g/L, Six Al sheets	[35]
50	80%	Current density 8 mA/cm², Reaction time 20 min, NaOH concentration 2 wt%, Fe–Fe	[36]
50	99.45%	Current density 2.6 mA/cm², Reaction time 17.75 min, Al–SS, pH 7, HNS dosage 6 g/L	this study

Conclusions

In this work, MB was removed from aqueous solution by EC using aluminium (anode) and stainless steel (cathode) coupled with HNS adsorption. Optimisation of removal efficiency was performed using response surface method based on a three-variable, three-level Box-Behnken design. Regression analysis revealed the good fit of the experimental data to a second-order polynomial model with an R^2 value of 0.9534 and an F value of 209.88. The ANOVA results showed that the effects of HNS dosage, reaction time, current density and combined effect of reaction time and current density were all significant to MB removal efficiency. The maximum removal efficiency of 99.45% was obtained under the following optimal parameters: adsorbent dosage of 6 g/L, current density of 2.6 mA/cm² and reaction time of 17.75 min. ANOVA results showed that reaction time possessed a low p value (<0.05) and a high F value (16.71), thereby implying that reaction time is the most significant factor affecting MB removal efficiency. The findings of this study showed that MB can be efficiently removed from aqueous solutions using EC/HNS technology. Future research on optimizing the proposed approach should be conducted on a large scale that considers energy consumption.

Acknowledgements

Conflict of Interest

The authors declare no conflict of interest.

References

1. DARDOURI S., SGHAIER J. Adsorptive removal of methylene blue from aqueous solution using different agricultural wastes as adsorbents. Korean J. Chem. Eng. **34** (4), 1037, **2017**.

2. DOĞAN M., ABAK H., ALKAN M. Biosorption of Methylene Blue from aqueous solutions by hazelnut shells: equilibrium, parameters and isotherms. Water Air Soil Pollut. **192** (1-4), 141, **2008**.

3. KUMAR K.V., RAMAMURTHI V., SIVANESAN S. Modeling the mechanism involved during the sorption of methylene blue onto fly ash. J. Colloid Interface Sci. **284** (1), 14, **2005**.

4. ZHOU C., WU Q., LEI T., NEGULESCU II. Adsorption kinetic and equilibrium studies for methylene blue dye by partially hydrolyzed polyacrylamide/cellulose nanocrystal nanocomposite hydrogels. Chem. Eng. J. **251**, 17, **2014**.

5. MISHRA S., KUMAR P. Attenuation of methylene blue dye during riverbank filtration through sandy aquifers. Water Environ. J. **29** (4), 507, **2015**.

6. WANG B., DONG B., XU M., CHI C., WANG C. Degradation of methylene blue using double-chamber dielectric barrier discharge reactor under different carrier gases. Chem. Eng. Sci. **168**, 90, **2017**.

7. SHESTAKOVA M., GRAVES J., SITARZ M., SILLANPÄÄ M. Optimization of $Ti/Ta_2O_5-SnO_2$ electrodes andreaction parameters for electrocatalytic oxidation of methylene blue. J. Appl. Electrochem. **46** (3), 349, **2016**.

8. SINGH J., YANG J.K., CHANG Y.Y., KODURU J.R. Fenton-like degradation of Methylene Blue by ultrasonically dispersed nano zero-valent metals. Environ. Processes **4** (1), 169, **2017**.

9. ZHANG Y., SHANG J., SONG Y., RONG C., WANG Y., HUANG W., YU K. Selective Fenton-like oxidation of methylene blue on modified Fe-zeolites prepared via molecular imprinting technique. Water Sci. Technol. **75** (3-4), 659, **2017**.

10. TRANDAFILOVIĆ L.V., JOVANOVIĆ D.J., ZHANG X., PTASIŃSKA S., DRAMIĆANIN M.D. Enhanced photocatalytic degradation of methylene blue and methyl orange by ZnO:Eu nanoparticles. Appl. Catal. B Environ. **203**, 740, **2017**.

11. KOBAYASHI D., HONMA C., MATSUMOTO H., TAKAHASHI T., KURODA C., OTAKE K., SHONO A. Kinetics analysis for development of a rate constant estimation model for ultrasonic degradation reaction of methylene blue. Ultrason. Sonochem. **21** (4), 1489, **2014**.

12. SECULA M.S., CAGNON B., OLIVEIRA T.F.D., CHEDEVILLE O., FAUDUET H. Removal of acid dye from aqueous solutions by electrocoagulation/GAC adsorption coupling: Kinetics and electrical operating costs. J. Taiwan Inst. Chem. Eng. **43** (5), 767, **2012**.

13. SECULA M.S., CRETESCU I., CAGNON B., MANEA L.R., STAN C.S., BREABAN I.G. Fractional factorial design study on the performance of GAC-enhanced electrocoagulation process involved in color removal from dye solutions. Materials **6** (7), 2723, **2013**.

14. CARVALHO H.P.D., HUANG J.G., ZHAO M.X., LIU G., DONG L.L., LIU X.J. Improvement of Methylene Blue removal by electrocoagulation/banana peel adsorption coupling in a batch system. Alex. Eng. J. **54** (3), 777, **2015**.

15. MOLLAH M.Y., SCHENNACH R., PARGA J.R., COCKE D.L. Electrocoagulation (EC)−science and applications. J. Hazard. Mater. **84** (1), 29, **2001**.

16. KOBYA M., GENGEC E. Decolourization of melanoidins by an electrocoagulation process using aluminium electrodes. Environ. Technol. **33** (21), 2429, **2012**.

17. GUVENC S.Y., OKUT Y., OZAK M., HAKTANIR B., BILGILI M.S. Process optimization via response surface methodology in the treatment of metal working industry wastewater with electrocoagulation. Water Sci. Technol. **75** (3-4), 833, **2017**.

18. ZHU M.J., YAO J., WANG W.B., YIN X.Q., CHEN W., WU X.Y. Using response surface methodology to evaluate electrocoagulation in the pretreatment of produced water from polymer-flooding well of Dagang Oilfield with bipolar aluminum electrodes. Desal. Water Treat. **57** (33), 15314, **2016**.

19. AVSAR Y., KURT U., GONULLU T. Comparison of classical chemical and electrochemical processes for treating rose processing wastewater. J. Hazard. Mater. **148** (1-2), 340, **2007**.

20. VIVEK N.N., GANESAN M. Use of adsorption using granular activated carbon (GAC) for the enhancement of removal of chromium from synthetic wastewater by electrocoagulation. J. Hazard. Mater. **16 1**(1), 575, **2009**.

21. DOĞAN M., ABAK H., ALKAN M. Adsorption of methylene blue onto hazelnut shell: Kinetics, mechanism and activation parameters. J. Hazard. Mater. **164** (1), 172, **2009**.

22. FERRERO F. Dye removal by low cost adsorbents: hazelnut shells in comparison with wood sawdust. J. Hazard. Mater. **142** (1-2), 144, **2007**.

23. DEMIRBAŞ Ö., KARADAĞ A., ALKAN M., DOĞAN M. Removal of copper ions from aqueous solutions by hazelnut shell. J. Hazard. Mater. **153** (1-2), 677, **2008**.

24. ZHU M.J., LIU R.P., CHAI H.K., YAO J., CHEN Y.P., YI Z.J. Hazelnut shell activated carbon: a potential adsorbent material for the decontamination of uranium(VI) from aqueous solutions. J. Radioanal. Nucl. Chem. **310** (3), 1147, **2016**.

25. WANG X., NI J., PANG S., LI Y. Removal of malachite green from aqueous solutions by electrocoagulation/peanut shell adsorption coupling in a batch system. Water Sci. Technol. **75** (8), 1830, **2017**.

26. LEAL D., MATSUHIRO B., ROSSI M., CARUSO F. FT-IR spectra of alginic acid block fractions in three species of brown seaweeds. Carbohydr. Res. **343** (2), 308, **2008**.

27. BARUAH S., DEVI A., BHATTACHARYYA K.G., SARMA A. Developing a biosorbent from *Aegle Marmelos* leaves for removal of methylene blue from water. Int. J. Environ. Sci. Technol. **14** (2), 341, **2017**.

28. YANG X., LIU H., HAN F., JIANG S., LIU L., XIA Z. Fabrication of cellulose nanocrystal from *Carex meyeriana* Kunth and its application in the adsorption of methylene blue. Carbohydr. Polym. **175**, 464, **2017**.

29. MIR A.A., AMOOEY A.A., GHASEMI S. Adsorption of direct yellow 12 from aqueous solutions by an iron oxide-gelatin nanoadsorbent; kinetic, isotherm and mechanism analysis. J. Clean. Prod. **170**, 570, **2018**.

30. ZHU J., WU F.C., PAN X.L., GUO J., WEN D. Removal of antimony from antimony mine flotation wastewater by electrocoagulation with aluminum electrodes. J. Environ. Sci. **23** (7), 1066, **2011**.

31. ZHU M.J., YAO J., QIN Z.H., LIAN L.N., ZHANG C. Response surface methodology approach for the

optimisation of adsorption of hydrolysed polyacrylamide from polymer-flooding wastewater onto steel slag: a good option of waste mitigation. Water Sci. Technol. **76** (3-4), 776, **2017**.

32. ASSÉMIAN A.S., KOUASSI K.E., DROGUI P., ADOUBY K., BOA D. Removal of a persistent dye in aqueous solutions by electrocoagulation process: modeling and optimization through response surface methodology. Water Air Soil Pollut. **229**, 184, **2018**.

33. TIR M., MOULAI-MOSTEFA N., NEDJHIOUI M. Optimizing decolorization of methylene blue by electrocoagulation using Taguchi approach. Desal. Water Treat. **55** (10), 2705, **2015**.

34. MOSTAFA A., ESMAIL G., MANSUR Z., SARA H. Efficient de-colorization of methylene blue by electro-coagulation method: comparison of iron and aluminum electrodes. Iran. J. Chem. Chem. Eng. **34** (1), 39, **2015**.

35. PANTORLAO W., CHANNEI D., KHANITCHAIDECHA W., NAKARUK A. Decolorization of methylene blue solution by electrocoagulation using aluminum electrodes. Chiang Mai J. Sci. **45** (5), 2238, **2018**.

36. MAHMOUD M.S., FARAH J.Y., FARRAG T.E. Enhanced removal of methylene blue byelectro-coagulation using iron electrodes. Egypt. J. Petro. **22** (1), 211, **2013**.